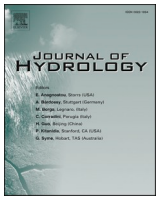
Journal of Hydrology 645 (2024) 132193



Contents lists available at ScienceDirect

Journal of Hydrology

journal homepage: www.elsevier.com/locate/jhydrol





Sensitivity of snow magnitude and duration to hydrology model parameters

Bhupinderjeet Singh [a,*], Tanvir Ferdousi [b], John T. Abatzoglou [c], Samarth Swarup [b], Jennifer C. Adam [d], Kirti Rajagopalan [a,*]

[a] Department of Biological Systems Engineering, Washington State University, USA
[b] Biocomplexity Institute, University of Virginia, Charlottesville, VA, USA
[c] Management of Complex Systems, University of California, Merced, CA, USA
[d] Department of Civil and Environmental Engineering, Washington State University, USA

ARTICLE INFO

This manuscript was handled by Marco Borga, Editor-in-Chief, with the assistance of Denis Ruelland, Associate Editor

ABSTRACT

Process-based hydrology models are critical for understanding streamflow and water supply under global change. However, these models require parameterization which introduces additional uncertainty into the models. The role that these parameters play in driving uncertainty is under-studied, especially for intermediary processes outside of streamflow. An important example in snowmelt dominant regions are intermediary processes related to snowpack accumulation and ablation. We examine the sensitivity of snow magnitude and duration to eleven parameters relevant to snow processes in the coupled crop-hydrology model VIC-CropSyst using a hybrid global–local Distributed Evaluation of Local Sensitivity Analysis approach. With the Pacific Northwest US as a case study, our specific research questions are: *(a) What is the sensitivity response of peak snow water equivalent (SWE) and snow duration and how does it vary in the parameter space? (b) What are the key drivers of the sensitivity response? and (c) Which of the most sensitive parameters can we immediately improve by leveraging existing data products*? Both target variables were sensitive to less than four of the eleven parameters. We found that peak SWE was most sensitive to either the precipitation partitioning temperature threshold or the albedo of new snow, depending on the geography and associated interplay between hydro-meteorological factors. In contrast, snow duration was primarily sensitive to the albedo of new snow and the albedo decay coefficient during snowmelt. Machine learning explainability workflows applied on the sensitivity response explained the model behavior and determined key geographic and hydro-meteorological drivers of the sensitivity response. Regions where the significant precipitation co-occurred with near-freezing temperature exhibited higher sensitivity of peak SWE to precipitation partitioning. In contrast, much colder high-elevation regions that have a delayed snowmelt-driven runoff when downward shortwave radiation is higher, displayed more sensitivity to albedo parameters. We also noted differences in the list of key parameters and in the level of sensitivity between our work and the limited comparable existing work. This highlights the need for comprehensive sensitivity analysis of snow metrics to become a routine component of hydrology model application studies in addition to streamflow. This is critical for us to better understand model behavior, identify key model parameters that can benefit from more dynamic representation in the models, and strategically improve models to best support decision-makers.

1. Introduction

Streamflow is the lifeline for a variety of societal needs such as irrigation, hydropower production, maintaining endangered fish species, recreation, and navigation. Hydrological models are commonly used to understand streamflow dynamics and manage water resources (Hall et al., 2024; Hamlet et al., 2013; Lee et al., 2011; Zhao et al., 2012). In many snow-dominant watersheds, such as in the Western United States, most streamflow originates as snowmelt (Li et al., 2017; Stewart et al., 2004). In these watersheds, snow dynamics are a critical component of hydrological model performance and applications.

The hydrological modeling community has made substantial progress in representing the complex natural system and snow dynamics within Land Surface Models (LSMs) by incorporating more physical processes and capturing interactions within the system (Clark et al., 2015; Lawrence et al., 2011; Maxwell and Miller, 2005; Niu et al., 2011;

* Corresponding authors.
E-mail addresses: bhupinderjeet.singh@wsu.edu (B. Singh), kirtir@wsu.edu (K. Rajagopalan).

https://doi.org/10.1016/j.jhydrol.2024.132193
Received 12 April 2024; Received in revised form 6 September 2024; Accepted 5 October 2024
Available online 15 October 2024
0022-1694/© 2024 The Authors. Published by Elsevier B.V. This is an open access article under the CC BY-NC-ND license (http://creativecommons.org/licenses/by-nc-nd/4.0/).

Qu and Duffy, 2007; Rigon et al., 2006). This shift from simple empirical models (Darcy, 1856; Horton, 1933; Richards, 1931) to process-driven LSMs (Liang et al., 1994; Niu et al., 2011; Regan et al., 2018; Vertessy et al., 1996) has become possible due to increased data availability and advancements in computational power, but has also led to increased parameterization that adds to model uncertainty.

In spite of widespread applications of LSMs, model sensitivity to parameters has primarily focused on streamflow (Chaney et al., 2015; Demaria et al., 2007; Liang and Guo, 2003; Lilhare et al., 2020; Melsen et al., 2016; Yeste et al., 2020), and uncertainties and model sensitivities related to several important processes (e.g., snow processes) remain unclear (Houle et al., 2017; Mendoza et al., 2015). This gap needs to be bridged to properly interpret simulated hydrological processes, quantify uncertainties in model output, attribute model-observation mismatch to the right factors, and identify priorities for model improvements, especially in snow-dominant watersheds. This is even more relevant in the current context where LSMs have a large number of parameters, many of which are non-measurable or come from limited in-situ or lab experiments (Demaria et al., 2007), and are often assumed to be static even though they should vary in space and time dynamically. Our overarching goal is to enhance our understanding of the sensitivity of snow processes in hydrology models. The specific research questions addressed are *(a) What is the sensitivity response of peak snow water equivalent (SWE) and snow duration and how does it vary in the parameter space? (b) What are the key drivers of the sensitivity response? and (c) Which of the most sensitive parameters can we immediately improve by leveraging existing data products?*

To address our research question, we utilize the *VIC-CropSyst* model (Malek et al., 2017), a coupled crop hydrology model where the hydrology aspects – including the snow model – come from a very widely used LSM, *Variable Infiltration Capacity (VIC model version 4.1.2.e;* Liang et al., 1994). The VIC hydrology model has been used in a large number of applications across the world related to streamflow forecasting (Anghileri et al., 2016; Mazrooei et al., 2021; Ossandón et al., 2022; Singh et al., 2023), snow modeling (Bhend et al., 2012; Li et al., 2017; Murillo et al., 2022; Schreider et al., 1997; Tang and Lettenmaier, 2010), climate change impact assessment (Dang et al., 2020; Guo et al., 2009; Hengade et al., 2018; Krysanova and Hattermann, 2017; Treesa et al., 2017; Yeste et al., 2021), and land-use change impact assessment (Carvalho et al., 2022; Garg et al., 2017; Hengade et al., 2018). Despite this wide application, only a handful of studies have focused on identifying the impact of model parameters on snow-related processes (e.g., Houle et al., 2017; Bennett et al., 2018b; Sepúlveda et al., 2022; Larabi et al., 2023). Moreover, some of these studies were conducted on limited domains or point locations (e.g., Houle et al., 2017 analyzed 5 SNOTEL stations, and Bennett et al., 2018b analyzed seven grids) which may inhibit understanding of processes across a broader hydroclimate regimes and limit the application of such parameters in novel hydroclimate space.

We perform a spatially-explicit parameter sensitivity analysis across all grid cells (0.0625° x 0.0625° spatial resolution) with non-negligible annual snow within the Pacific Northwest US. Our geographic focus has a large climatic and topographic diversity and is a much larger spatial extent than considered in recent work (e.g., Sepúlveda et al. (2022) and Larabi et al. (2023)). We selected 11 snow-related parameters in the VIC-CropSyst model (including a few not considered by Sepúlveda et al., (2022) and Larabi et al. (2023)), many of which are space–time invariant and hardcoded in the model, as historically they were not easily measurable. We perform a sensitivity analysis of two target variables, peak SWE, and the snow duration, utilizing a hybrid local–global Distributed Evaluation of Local Sensitivity Analysis (DELSA) approach (Rakovec et al., 2014).

When sensitivity analyses are performed to inform calibration exercises, target variables are often the model performance metrics (e.g., Houle et al., 2017; Yeste et al., 2023). This is because a key application of sensitivity analysis is to facilitate identification of a subset of key parameters and parameter ranges that most influence calibration results and model performance improvement. This is especially important in high-dimensional multi-objective calibration contexts to lower the complexity and computational requirements of the calibration effort (Rakovec et al., 2014; Song et al., 2015; Yeste et al., 2023). However, sensitivity analysis is also useful to understand model behavior (e.g., Larabi et al., 2023; Melsen and Guse, 2019; Sepúlveda et al., 2022), evaluate the benefits of increasing model complexity (Rosolem et al., 2012; Saltelli et al., 1999; Van Werkhoven et al., 2008), identify priority areas for new data collection (Fienen et al., 2010; Tonkin et al., 2007; Weerts et al., 2001), and as a diagnostic tool to investigate model performance in new context such as climate change (Karimi et al., 2022). When sensitivity analyses in applied in these contexts, the target variable is not typically performance metrics of the variables of interest, but the variable itself.

In these contexts, sensitivity analysis results are most useful and actionable when they are accompanied by explanations of the drivers of the sensitivity response. For this, we apply a novel machine learning workflow to the sensitivity response, adapting the SHapley Additive exPlanations (SHAP) game-theoretic methodology used for machine learning model explainability (Lundberg and Lee, 2017), to facilitate the identification of key drivers and better understand complex model behavior. This method works better than simple correlation analysis used in prior work as it can account for the non-linear and non-monotonic ways in which drivers impacts the target variables, and also quantifies the additional explainability offered by a driver after accounting for contributions from other drivers.

While we focus on the VIC-CropSyst model as a case study, the insights are expected to be relevant more broadly in the context of other hydrology models, which although can vary widely in complexity and model structure, also include a common set of processes related to snow accumulation and melt (Valéry et al., 2014) that are typically parameterized.

2. Methodology

2.1. Study domain

The Pacific Northwest includes the Columbia River basin (CRB) that covers multiple states in the US and Canada with an area of about 670 thousand km^2, and coastal regions in the US (Fig. 1a). It contains multiple snow-dominant watersheds that regularly experience water scarcity issues, sometimes as a result of a mismatch in the timing of water supply and demand (Hall et al., 2024). There is high stakeholder interest in better forecasts of snowpack and streamflow for decision-making in the basin. These factors make the study domain an excellent case study for understanding snow model sensitivity and improving model performance. The region consists of areas with diverse climatic conditions ranging from arid, temperate, to cold climate classes (Beck et al., 2018). Precipitation is strongly influenced by the topography, with the western Cascades receiving more than 3000 mm/year and the eastern Rockies receiving relatively lower precipitation. As this study focuses on quantifying the impact of model parameters on the snow processes, we constrained our analysis to grids with mean April 1st SWE $>$ 5 mm, which led to 12,284 grid cells in the region covering 442,224 km^2 covering a broad elevation range (Fig. 1b-c).

2.2. Input dataset

We use the input datasets and the calibrated VIC-CropSyst model from recent work (Rajagopalan et al., 2018) updated in (Hall et al., 2024) in which inputs to the model were gridded meteorological datasets, soil characteristics, vegetation characteristics, elevation, and land cover parameters. Historical gridded meteorology input is the gridMET observational data product (Abatzoglou, 2013), which is available at daily high-spatial resolution (~4-km, 1/24th degree) covering the

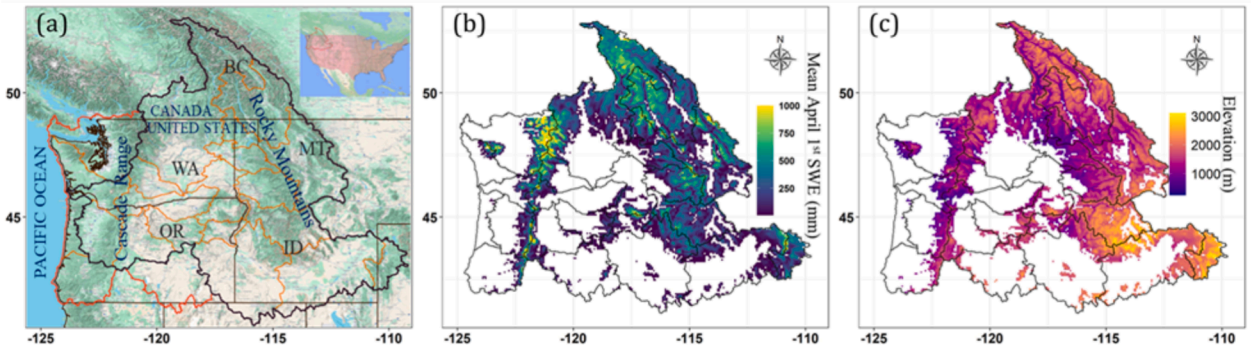


Fig. 1. (a) Basin map of the Pacific Northwest (red boundary) including the Columbia River basin (CRB) (black boundary) covering multiple states in the US and Canada. (b) shows average April 1st modeled SWE (period 1979–2015) for selected grids and (c) Spatial map showing the distribution of mean elevation. Note that grids with average April 1st SWE > 5 mm were selected.

Contiguous United States from 1979 to present. The gridMET dataset provides eight daily primary climate variables: precipitation accumulation, maximum and minimum temperature, specific humidity, downward surface shortwave radiation, wind velocity, and maximum and minimum relative humidity. The gridMET product was re-gridded to the 0.0625° VIC-CropSyst resolution via linear interpolation. For the Canadian portion, we used the similar variables available from (Livneh et al., 2013)) and estimated others (e.g., relative humidity and radiation) within the model. The soil parameters are based on the STATSGO2 (Staff, 2014) soil survey database which is provided by USDA NRCS. The crop land cover parameters consist of two data sources: the Washington State Department of Agricultural Land Use Layer (WSDA, 2018) for Washington State, and United States Department of Agriculture Cropland Data Layer (USDA-NASS, 2016) for other states in the United States. For the Canadian portion of CRB, soil data was used from Elsner et al. (2010). This dataset is based on Maurer et al. (2002), further developed as part of the Land Data Assimilation System (LDAS; Mitchell et al., 2004) project.

2.3. VIC-CropSyst model and calibration

The coupled hydrology-agricultural model, VIC-CropSyst (Malek et al., 2017) is a dynamic coupling between (a) the Variable Infiltration Capacity (VIC) model (Liang et al., 1994) version 4.1.2.e, a large-scale hydrological model that considers the water and energy balance to simulate the infiltration, snow accumulation and melt, baseflow, and runoff processes, and (b) the cropping systems model, CropSyst, which can dynamically grow crops considering a suite of management conditions (Stockle et al., 1994; Stöckle et al., 2003). VIC-CropSyst runs at a 0.0625° spatial resolution – where sub-grid lateral flow is assumed to be less relevant and not simulated – and at a daily time step. The model considers a spatially-explicit grid-level representation of soil characteristics, weather, vegetation, and crop types. Sub-grid variability is considered statistically, with fractions of areas within a grid associated with multiple elevation bands, vegetation, and crop types. Multiple elevation zones provide a more realistic simulation of real-world systems, especially in the mountainous regions where snow dynamics are relevant. Evaporation and transpiration are parameterized using the Penman-Monteith equation, which is applied separately to vegetation classes and bare soil. Just for the crop vegetation class, crop growth and actual evapotranspiration are dynamically calculated at a daily time step. The fluxes, mainly surface runoff, baseflow, and evapotranspiration, are calculated for each vegetation class and then added for each grid weighted by the fractional area covered by each vegetation class.

The snow sub-model solves for mass and energy balance to account for accumulation and ablation of snow in the canopy and the ground surface. Andreadis et al. (2009) provide a detailed description of the processes involved in the snow model. Briefly, the canopy interception of snow is a function of the leaf area index (LAI), and canopy storage of snow is a function of the LAI and meteorological variables. The ground snowpack is simulated in two-layers, a thin surface layer and thick deeper layer. The energy exchange between the atmosphere, land canopy, and snowpack happens only at the surface layer. Albedo, affecting reflectance at the surface layer, decays with age with different decay functions in the melting and accumulation phases. At every timestep, the model calculates how much precipitation is added to the snowpack and then calculates all mass and energy fluxes. The precipitation phase partitioning is determined using a simple linear scaling between a lower-bound temperature, below which all precipitation falls as snow, and an upper-bound temperature, above which all precipitation falls as rain. If the net energy balance is positive, then melt occurs, and if the amount of excess water exceeds the liquid water holding capacity of the surface or deep pack layer, then the water is released to the soil as snowpack outflow. In case of a negative energy balance, all liquid water (if present) freezes. Parameters accounting for canopy coverage, albedo of new snow and how it decays over time, snow density, snow surface roughness, the liquid water holding capacity, and temperature threshold assumptions for precipitation partitioning are all important in the snow model function. With the exception of LAI, these parameters are assumed to be spatiotemporally constant based on limited observations, and the snow model can be sensitive to these assumptions. One limitation of this snow model is that it does not account for wind-blown redistribution of snow, though this aspect matters more at smaller spatial scales and is likely less relevant at the larger scales of the VIC-CropSyst model.

For this study, we utilize the VIC-CropSyst model calibrated as part of Hall et al. (2024). The model was calibrated for five soil parameters using automatic calibration based on the multi-objective complex evolution (MOCOM-UA) global optimization method. All other parameters including snow-related parameters considered in this study were set to default values and were not part of the calibration process. Therefore, potential interactions between soil and snow parameter values are also ignored. Six streamflow performance metrics were used as objective functions for calibration: Nash Sutcliffe efficiency (NSE) of monthly runoff, ln (NSE) to account for low and high flows, relative bias in annual flow, coefficient of determination (R^2), absolute average peak flow difference, and root mean square error. Negative values are used for NSE, ln (NSE) and R^2 as high values are preferable for these metrics. From the final pareto front, the parameter set with the maximum average of NSE and ln(NSE), constrained to the value being greater than 0.5, is chosen as the final calibrated parameter combination. The calibration was conducted in a nested approach, in which grids for upstream stations are calibrated first, followed by remaining grids at the downstream station until the whole watershed is calibrated. Crop irrigation is turned off in these VIC-CropSyst simulations to capture natural settings. Calibration results can be found in Adam et al. (2022).

Given that this work focuses on the snow dynamics that come from the VIC snow model, the sensitivity analysis performed here will not be impacted significantly by the CropSyst part of the model which handles crop dynamics. However, rather than running just the VIC model, we run the VIC-CropSyst model as the streamflow calibration was performed on this coupled model version and factors such as dynamic crop LAI will have had some influence on the streamflow as opposed to static monthly LAIs assumed in the VIC model for cropland areas. In general, we would expect the snow sensitivity analysis from the VIC-CropSyst model to be largely similar to that of the VIC model version integrated into the coupled model.

2.4. Sensitivity analysis approach

Many sensitivity analysis approaches and methods exist (Song et al., 2015). One distinction is global versus local sensitivity analysis where global analysis (Saltelli et al., 2008; Sobol, 2001) prioritizes identifying overall model sensitivity across the full parameter space, including non-linear relationships and interactions. This requires large samples across the parameter space, typically over 10,000 (He et al., 2011; Houle et al., 2017; Rakovec et al., 2014), which can lead to prohibitively high computational needs (Wainwright et al., 2014; Bennett et al., 2018b). Local analysis, in contrast, while computationally cheap, only quantifies the effect of changes in a single parameter at a time while keeping other parameters constant. Unlike global analysis, sensitivities are therefore not evaluated on multiple samples of parameter sets. Hybrid local–global sensitivity analysis methods such as Distributed Evaluation of Local Sensitivity Analysis (DELSA; Rakovec et al., 2014) also exist. They prioritize identifying how sensitivities vary across the parameter space, while still considering the global parameter space, although to a lesser extent than global sensitivity analysis. To do this, these approaches taker fewer samples in the parameter space than global analysis (a few hundred samples rather than thousands) and complement it with additional simulations of local sensitivity (e.g., Melsen et al., 2016; Melsen and Guse, 2021; Mendoza et al., 2015; Sepúlveda et al., 2022; Yeste et al., 2023). As a result, their computational requirements tend to be lower. We utilize this hybrid DELSA approach for this study.

We apply the DELSA method across the 12,284 grid cells across the study area for two target variables: (a) differences in the accumulated annual maximum SWE, which has been widely used to estimate the maximum amount of water available through the snowpack, and (b) differences in length of the snow season that is defined as the number of days with snow on the ground (the number of days SWE $>$ 1 mm). We consider the sensitivity of these target variables to 11 parameters directly related to snow processes in the model. Feasible parameter boundaries were determined from existing literature (Table 1).

Rakovec et al. (2014) provides a detailed explanation of the DELSA methodology, which we briefly summarize here. Consider a model f, with a vector of parameter values $\theta = [\theta_1, \theta_2, \cdots, \theta_k]$ with a length of k. Typically, a model calibration process determines optimal values for the k parameters (θ^*) based on some model performance metric. In local sensitivity analysis, the model output with these calibrated parameter values ($\theta = [\theta_1^*, \theta_2^*, \cdots, \theta_k^*]$) is considered as the base run. Then, subsequently, one parameter is perturbed by a 1 % while holding the other parameters constant to get perturbed value of the model output. Then the change in model output is compared to the base run to compute the local sensitivity of the target variable, ψ, to the perturbed parameter (Eq. (1).

$$\frac{\partial \Psi}{\partial \theta_j}|\theta^* = \frac{\Psi(\theta_j^*) - \Psi(\theta_j^* + (0.01\theta_j^*))}{0.01 \times \theta_j^*}, j \in 1, 2, \cdots k \quad (1)$$

In the DELSA method, this local sensitivity analysis is computed for several feasible parameter sets distributed across the parameter space rather than just the calibrated base run parameter set. Given a sample point θ^* in the parameter space, the local sensitivity is estimated by computing a gradient using a forward finite difference approach with a 1 % change in parameter value. This sensitivity across multiple sets of parameters mimics the global sensitivity analysis considering the full parameter space. The hybrid local–global sensitivity is quantified as a first-order sensitivity measure for the j^{th} parameter estimated at each sample point (S_j^L) as

$$S_j^L = \frac{(\frac{\partial \psi}{\partial \theta_j}|\theta^*)^2 s_j^2}{V_L(\theta^*)} \quad (2)$$

Here, s_j^2 is the variance from the uniform distribution i.e., $1/12(\theta_{j,max} - \theta_{j,min})^2$ and $V_L(\theta^*)$ is the linearized local variance.

$$V_L(\theta^*) = \sum_{j=1}^{k} (\frac{\partial \psi}{\partial \theta_j}|\theta^*)^2 s_j^2 \quad (3)$$

The first-order sensitivity varies between zero and one, and the sum of the sensitivities across all parameters equals one for each sampling point. The first-order sensitivity of a target variable to an individual parameter provides the relative contribution of that parameter in explaining the total variance in the target variable. Each grid and parameter set has a first-order sensitivity for each parameter, and a cumulative distribution curve of grids with different first-order sensitivities can be created for each parameter set. The area above each of these curves (RC_j^L) can be computed as in Eq. (4) where $F(S_j^L)$ is the cumulative frequency curve of S_j^L for each parameter set. High values of the area above the curve are indicative of a larger number of grids with high sensitivities for a parameter, and a large spread in the areas is indicative of a large variation in sensitivity across the parameter space.

$$RC_j^L = 1 - \int_0^1 F(S_j^L) dS_j^L \quad (4)$$

Table 1
VIC-CropSyst model parameter list and parameter ranges considered in this study. Information from Sepúlveda et al., 2022 is modified based on other references as noted.

Parameter	Description	Units	Min	Max	References
MIN_RAIN_TEMP (Trmin)	Minimum temperature at which rain can fall)	°C	−3	0	Melsen and Guse, 2021
MAX_SNOW_TEMP (Tsmax)	Maximum temperature at which snow can fall	°C	0	3	Melsen and Guse, 2021
NEW_SNOW_ALB (NSA)	Albedo of new snow	–	0.7	0.99	Mendoza et al., 2015
SNOW_ALB_ACCUM_A (SACC_A)	Albedo decay coefficient during accumulation	–	0.88	0.99	Mendoza et al., 2015
SNOW_ALB_ACCUM_B (SACC_B)	Albedo decay exponent during accumulation	–	0.5	0.75	–
SNOW_ALB_THAW_A (STHA_A)	Albedo decay coefficient during melt	–	0.66	0.98	Mendoza et al., 2015
SNOW_ALB_THAW_B (STHA_B)	Albedo decay exponent during melt	–	0.4	0.6	–
NEW_SNOW_DENSITY (NSD)	Density of new snow	kg/m^3	25	150	Houle et al., 2017
LIQUID_WATER_CAPACITY (LWC)	Liquid water holding capacity	–	0.02	0.15	Houle et al., 2017
SNOW_ROUGNESS (ROUGH)	Surface roughness of snowpack	–	0.0005	0.05	–
LAI_ADJUSTMENT (LAI)*	Leaf area index of vegetation type indicative of canopy cover	–	0.1	1.16	Dorman and Sellers, 1989; Myneni et al., 1997

*This parameter varies monthly and by landcover type; therefore, its sensitivity is analyzed based on multipliers.

Given the high number of potential parameter combinations across eleven parameters (Table 1), we use a Latin hypercube sampling (LHS) to obtain a sample of 100 points (base runs) across the parameter space following the approach of (Melsen and Guse, 2021, 2019). We acknowledge that this set of base runs, while intended to largely capture the sensitivity response in the global parameter space, may miss parts of the sensitivity range given it a smaller sub-sample. Each parameter range is assumed to be uniformly distributed for sampling, and we sample uniformly from the 11-dimensional hypercube. Then, for individual base runs, local sensitivity analysis was computed by perturbing each parameter by 1 %, which results in a perturbation of individual parameters 100 times. The computational cost of applying the DELSA method at each grid is $N_l(k + 1) = 1200$ runs, where N_l is the number of samples of parameter sets (100) and k is the number of parameters considered (11). This cost is an order of magnitude lower than the computational costs of global sensitivity analysis (typically $>$ 10,000 simulations).

2.5. Explainability of the sensitivity response

The term "*explainability*" is typically used in the context of black-box machine learning models and not process-based models. However, while process-based hydrology models are inherently explainable, the large numbers of parameters and processes in them, and the large amounts of simulation outputs produced by them make it challenging to interpret model behavior (Ferdousi et al., 2023) and results of sensitivity analyses. Therefore, approaches that are being developed to explain the behavior of black-box machine learning models (Lundberg and Lee, 2017) can be useful when applied in the context of explaining biophysical model behavior as well (e.g. Ferdousi et al., 2023). We utilize such a framework to explain the sensitivity response. Our goal here is to determine the features that play the most significant role in driving the observed differences in the shapes of the sensitivity curves. The approach involves three steps. The first involves an unsupervised clustering of the sensitivity responses to get broad groups of sensitivity responses in the multi-dimensional parameter space. This is followed by supervised clustering of these groups to identify drivers of membership (or non-membership) in each sensitivity response group. Finally, a feature importance analysis determines the most influential drivers in determining sensitivity response groups. This framework will work better to capture the non-linear and non-monotonic ways in which the features impact the target variable; an aspect that will be missing if simple correlation analysis is performed between the features and the target variables. Details of the three steps involved in this approach are further explained below.

2.5.1. Spatial clustering of grids based on the sensitivity response

We first applied a K-means unsupervised clustering algorithm (Forgy, 1965) using an Euclidean distance metric to classify the grid cells based on their sensitivity response. The sensitivity matrix had an initial dimension of 12,284 by 1100, representing 12,284 grids and 1100 first-order sensitivity values across different parameter sets (11 parameters * 100 sets). Due to the high dimensionality (1100) of the response vector of each grid, which is not conducive for clustering, we conducted dimension reduction. Initially, we eliminated insensitive parameters, defined as those with a mean first-order sensitivity below 0.05 across all simulations (based on Results section 3.1). This process left us with four parameters: Tsmax, Trmin, NSA, and LAI, reducing the dimension of the response vector from 1100 to 400. We then applied Principal Component Analysis to this to further reduce dimensions. We retained principal components (PCs), explaining 85 % of the total variance. This corresponded to 200 PCs and the final matrix for K-mean clustering had dimensions of 12,284 grids by 200 PCs. This dimensionality reduction not only enabled efficient training but also reduced noise and addressed multicollinearity issues by transforming correlated variables into uncorrelated components.

2.5.2. Drivers explaining the similarities and differences in the sensitivity response across identified classes

After the unsupervised clustering was completed, we performed an Extreme Gradient Boosting (XGBoost) supervised classification to develop a prediction model for the sensitivity-response classes determined in section 2.5.1. XGBoost is a scalable gradient-boosted tree algorithm. As potential prediction features, we used geographically-varying characteristics that can also be physically linked to climate characteristics, as well as meteorological variables. These include multiple soil, topographic, and meteorological variables (annual precipitation, sum of fraction of winter precipitation) and Koppen climate classes (Table S2). We computed the Pearson correlation coefficient between the features and dropped one parameter if a pair showed a Pearson correlation coefficient value of more than 0.5. While XGBoost is robust to multicollinearity, it can lead to issues while interpreting feature importance in the explainability analysis described in the next paragraph. After an iterative process of computing correlation and dropping features, we finalized 21 features (Table S1; see Figure S3 for correlation between finalized features). Using the shortlisted features and the sensitivity-response clusters, we trained the XGBoost classifier. The 12,284 grid points were split into 80 % training and 20 % testing sets. For the XGBoost classifier's hyperparameters, we set the maximum tree depth to 7, 140 estimators, minimum child weight of 10, and a learning rate of 0.1.

We then utilized a SHapley Additive exPlanations (SHAP) approach (Lundberg and Lee, 2017) to explain the sensitivity response class predictions of the XGBoost model via a feature importance analysis. SHAP is based on Shapley values, which are a game-theoretic approach to fairly apportion the predictive capability of a model among features. These values are calculated for every instance (row) in the data. For a particular data instance, the Shapley value for a particular feature can be interpreted as the marginal contribution of that feature to the difference between the predicted value of that instance and the average prediction, given the current set of other feature values. Each feature's marginal contribution value is calculated and averaged across all potential permutations of features. Features with larger absolute average Shapley values are more important than others. SHAP creates an aggregate global feature importance plot from the individual Shapley values and a summary plot which combines feature importance with feature effects and gives indications about the nature of the relationship (magnitude and direction) between a feature and the prediction. We used the shap.TreeExplainer() from the Python SHAP package (Lundberg et al., 2020), which is a computationally efficient way to perform SHAP analysis on tree-based models.

2.6. Simulation workflow

The entire workflow has been summarized in Fig. 2, outlining the three main objectives that have been addressed in this study. Section (a) quantifies the first-order sensitivity of target variables (peak SWE and snow duration) to the 11 snow-related parameters in the VIC-CropSyst model using the DELSA approach. Section (b) identifies the regions/classes exhibiting similar sensitivity responses using unsupervised K-means clustering based on the first-order sensitivity response of the target variable. Section (c) focuses on identifying the key drivers explaining the different classes of sensitivity response.

3. Results

Subsections 3.1 and 3.2 describe the DELSA first-order sensitivities for the peak SWE and snow duration target variables. Subsection 3.3 classifies sensitivity responses into similar groups and 3.4 identifies the features that explain group membership.

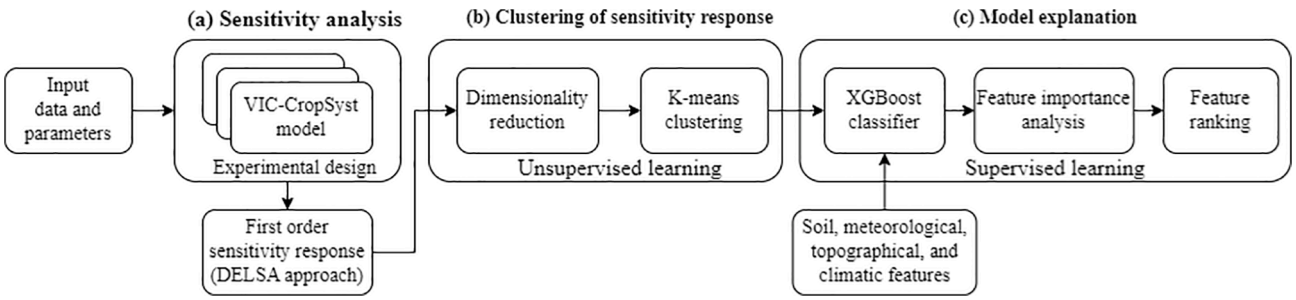


Fig. 2. The general framework for explainability of sensitivity response and parameter ranking of complex simulation models.

3.1. DELSA first-order sensitivities for peak SWE

Of the 11 parameters considered, overall, the highest first-order sensitivity of peak SWE was to the Tsmax parameter (Fig. 3a and Figure S1). This parameter, which relates to temperature thresholds that partition precipitation into rain and snow, also has the largest variations in first-order sensitivities across the parameter sets (the largest box plot length in Fig. 3a and largest variation across the hundred lines in Fig. 3b). In addition, the LAI, NSA, and Trmin parameters also contributed to the first-order sensitivities of Peak SWE, although at lower levels than Tsmax. For the NSA and Trmin parameters, there were very minimal variations in sensitivity across the parameter space (tight box plot in Fig. 3a and minimal spread across the lines in Figs. 3c and 3d), indicating that the sensitivity of peak SWE to these two parameters do not depend as much on the values of the other parameters and the outcomes of local sensitivity analysis will likely not be that different from a global sensitivity analysis. Peak SWE showed negligible first-order sensitivities to the other seven parameters (Fig. S1).

There are variations in sensitivities across the target variable space (Fig. S4). Sensitivities are similar to those described above when peak SWE values are less than 1000 mm, where most data points (~96 %) in the target space fall (Fig. S5). However, at higher peak SWE values both higher sensitivities and higher variations in sensitivities across the parameter space exist for NSA and STHA_A parameters rather than the Tsmax parameter.

3.2. DELSA first-order sensitivities for snow duration

Similar to peak SWE, non-negligible relative contribution to first-order sensitivity of snow duration also came only from four of 11 parameters, although the specific parameters and level of sensitivity were different (Fig. 4a and Fig. S2). In contrast to peak SWE, the snow duration was sensitive to NSA, STHA_A, LAI, and Tsmax parameters, with the highest sensitivity to the NSA parameter (Fig. 4a). NSA is the albedo parameter of new snow that controls the fraction of radiation that is reflected by new snow, impacting the energy exchange between the atmosphere and the surface layer of the snowpack (Andreadis et al., 2009). STHA_A is the parameter representing albedo decay coefficient during the melting phase in the albedo decay function. Overall, in contrast to peak SWE, which is relatively most sensitive to the partitioning of precipitation into rain and snow, the snow duration is more sensitive to the albedo parameters.

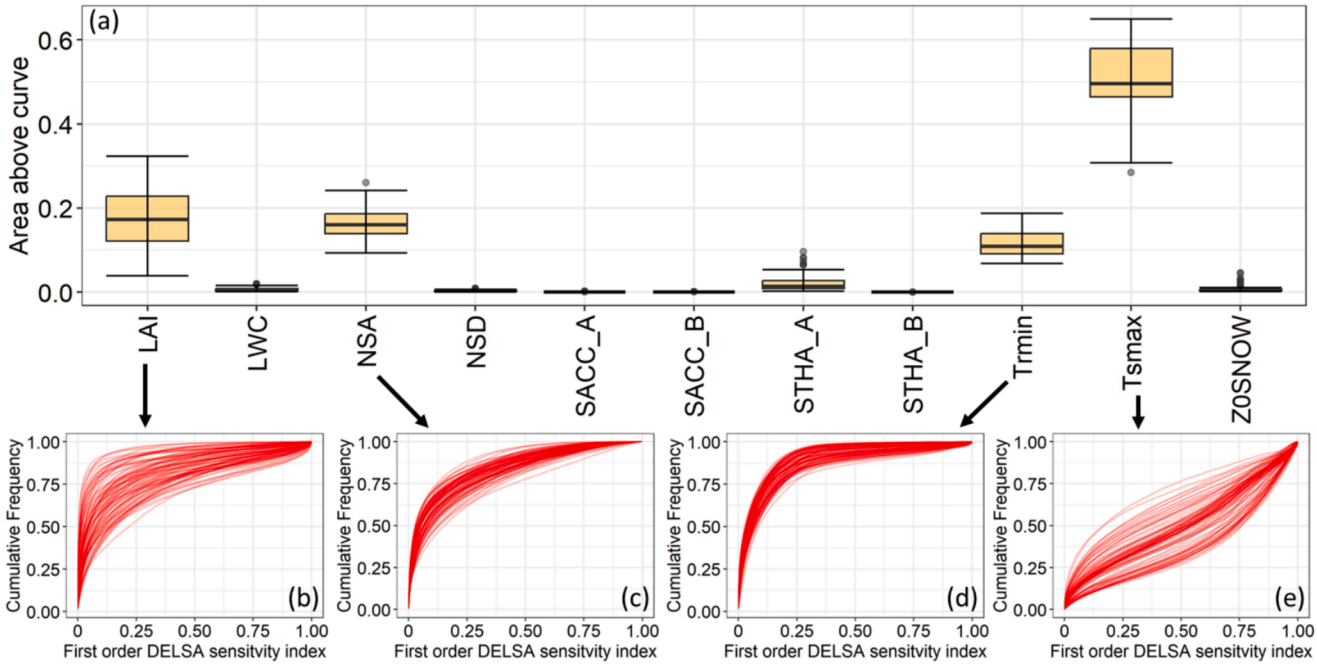


Fig. 3. The top panel (a) provides the first-order sensitivities of peak SWE to all 11 parameters tested. This is the area above the cumulative frequency curves in the bottom part (b-e). The range in the box plot comes from 100 *areas above the curve* resulting from the 100 lines in each panel of part (b-e). The bottom panel displays the cumulative frequency plot for the 4 parameters (b) LAI, (c) NSA, (d) Trmin, and (e) Tsmax with non-negligible contribution to peak SWE's sensitivity in part (a). There are 100 lines in each panel corresponding to the 100 sets of parameter values simulated. For a given parameter set, the Y-axis corresponds to the cumulative fraction of grids displaying a given level of sensitivity (X-axis). For a particular parameter, lines that are spread out indicate a large variation in the sensitivity of peak SWE to that parameter based on the values of other parameters in the global parameter space.

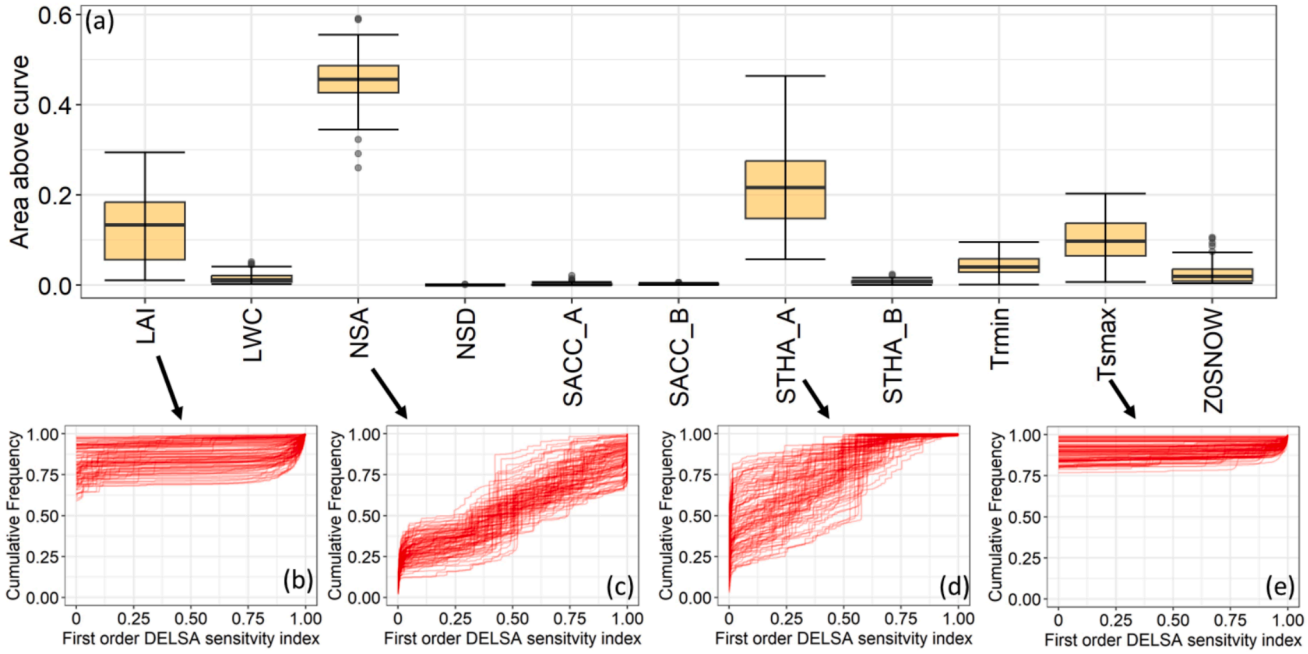


Fig. 4. The top part (a) provides the first-order sensitivities of snow duration to all 11 parameters tested. This is the area above the cumulative frequency curves in the bottom part (b-e). The range in the box plot comes from 100 *areas above the curve* resulting from the 100 lines in each panel of part (b-e). The bottom panel displays the cumulative frequency plot for the 4 parameters (b) LAI, (c) NSA, (d) STHA_A, and (e) Tsmax with the non-negligible contribution to snow duration's sensitivity in part a). There are 100 lines in each panel corresponding to the 100 sets of parameter values simulated. For a given parameter set, the Y-axis corresponds to the cumulative fraction of grids displaying a given level of sensitivity (X-axis). For a particular parameter, lines that are spread out indicate a large variation in the sensitivity of snow duration to that parameter based on the values of other parameters in the global parameter space.

Additionally, snow duration has zero first-order sensitivity to LAI and Tsmax for a majority of grids for most parameter sets. Figs. 4b and 4e are essentially flat lines at the top of the plot, indicating zero first-order sensitivity of snow duration to these two parameters for over 75 % of the grids with essentially no regional variation in response.

There are variations in sensitivities across the target variable space (Fig. S6). While the NSA parameter has the highest first order sensitivity consistently across the full target space, the relative sensitivity of STHA_A is higher for higher snow durations, and those of LAI and Tsmax are higher for lower snow durations.

3.3. Identifying areas with a similar sensitivity response

This and the following section focuses only on the peak SWE's parametric sensitivity, given we are interested in regional controls. There is no regional variation (across grids) in the first-order sensitivity of snow duration for 2 out of the 4 sensitive parameters, as noted in section 3.2. So, we performed an unsupervised clustering of all the grids in the study area based on their first-order sensitivities of peak SWE across the parameter space. This resulted in four clusters of grids (Fig. 5a). The distribution of grids across these clusters is as follows:

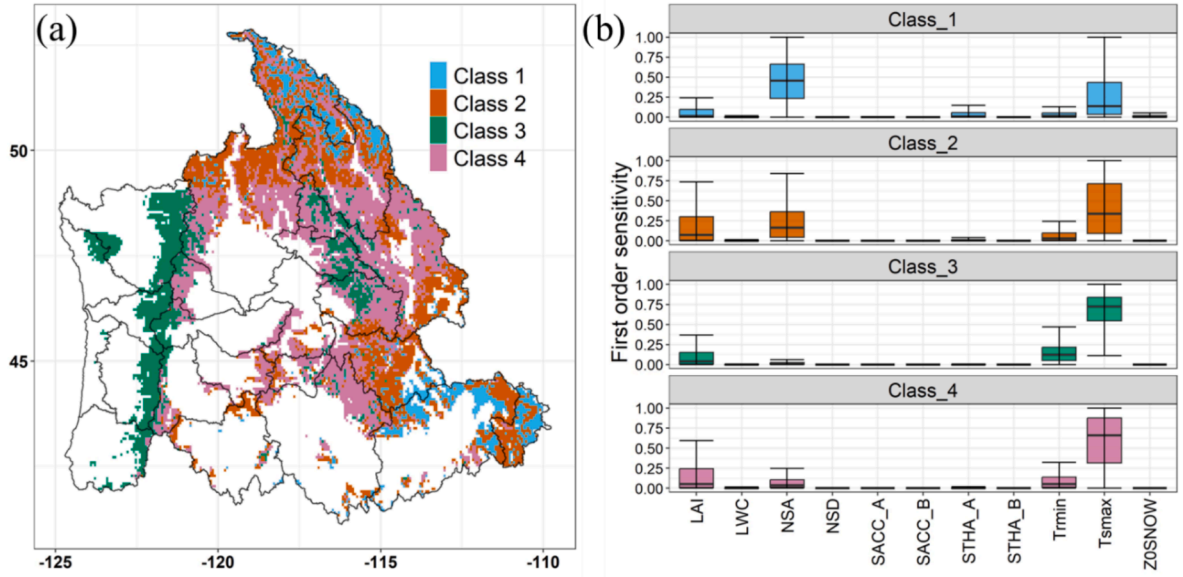


Fig. 5. (a) Four classes of grid cells based on unsupervised K-Means clustering. Each grid cell is depicted as a point on the map with a color corresponding to its class (b) Boxplot showing the distribution of first-order DELSA sensitivity indices of the peak SWE to 11 parameters by class.

Class 1 (2,164 grids), Class 2 (3,689 grids), Class 3 (1,554 grids), and Class 4 (4,877 grids).

Although unsupervised clustering identified four distinct classes, the grids broadly fall into two main groups. The first group comprises Classes 3 and 4, where the peak SWE exhibits higher sensitivity to the rain-snow partitioning temperature threshold (Tsmax) and lower sensitivities to other parameters, including NSA (Fig. 5b). These classes are primarily situated in the lower elevation Cascades and mid-Rockies (Fig. 5a and Fig. 1). The second group consists of Classes 1 and 2, which have grids with higher sensitivity to the NSA parameter than the other classes (Fig. 5b). The grids in these groups are primarily located in the high-elevation areas of the Rockies (Fig. 5a and Fig. 1). Within the first group, the major difference between Class 3 and 4 is relatively higher and lower sensitivities to LAI and Tsmax, respectively, for Class 4 compared to Class 3. The main difference between Classes 1 and 2, is that peak SWE in Class 2 exhibits a lower level of sensitivity to the NSA parameter as compared to Class 1 and exhibits higher sensitivity to the LAI and Tsmax parameters.

3.4. Identifying features that distinguish the sensitivity response classes

3.4.1. Classifier results

The trained XGBoost classifier had an overall macro F1-score (where the F1-score of each of the four classes is given equal weight) of 0.78 on the test dataset (Table 2). While class 3 and 4 have similar F1-scores (~0.82), class 3 has a higher precision (0.90) and lower recall (0.76) while class 2 has a higher recall (0.84) and lower precision (0.77). That is, 90 % of class 3 members are correctly predicted as class 3 (low false positives), while 84 % of predicted class 4 members were actually class 4 (low false negatives).

The 21 features used for classification were then ranked based on their SHAP values (Fig. 6a), which indicates each feature's relative influence on cluster membership. Features corresponding to topographical, meteorological, and soil characteristics all influenced the sensitivity surface of clusters. The fraction of precipitation occurring in winter exerts the highest influence in identifying classes 2, and 3, with the highest influence for class 3, while elevation exerts the highest influence for classes 1 and 4 (Fig. 6a). The second highest influence is exerted by annual precipitation for class 3, elevation for class 2, and fraction of precipitation in winter for classes 1 and 4. The soil characteristics (e.g., init_moist0, Clay0, and Wpwp_FRACT0) were not the most influential for any class, but they did contribute some additional information that helped explain class membership, especially for the grids in class 3 in the Cascades. This was similar for some soil parameters, which are important calibration parameters for streamflow as well (e.g., b_infilt, Dsmax, Ws), implying that streamflow calibration can play a role in affecting modeled peak SWE sensitivity. The Koppen climate classes played a minor role in identifying cluster membership, likely because some of the defining climate variables are already considered as separate variables (e.g., fraction of annual precipitation falling in winter directly corresponds to whether or not summers are dry in a region, one factor that goes into the Koppen classification).

For a better understanding of the direction in which these features influence clustering, we plotted the individual feature SHAP values for each of the four classes (Fig. 6b-e). Class 3 and 4, with higher classification accuracies (Table 2), are considered first.

A high fraction of precipitation in winter, high annual precipitation, and relatively lower elevation led to a sensitivity response representative of class 3 (Fig. 6d). Relatively lower elevation, a high fraction of precipitation in winter, and low annual precipitation lead to a sensitivity response representative of class 4 (Fig. 6e). Relatively higher elevation, lower winter precipitation, and lower annual precipitation lead to the sensitivity surface representative of classes 1 and 2 (Fig. 6b and 6c). Classes 1 and 2 had a mix of effects for the features, which is also reflected in their low accuracy metrics (Table 2).

Table 2
Summary of the XGBoost classification of grid cell clustering. N is the number of test samples.

Class	Color	Precision	Recall	F1-score	N
1	Blue	0.78	0.69	0.73	281
2	Orange	0.74	0.76	0.75	736
3	Cyan	0.90	0.76	0.82	482
4	Pink	0.77	0.84	0.81	958
macro avg. accuracy		0.80	0.77	0.78	2457
weighted avg accuracy		0.79	0.78	0.78	2457

3.4.2. Additional explanation of the variation across classes

The similarities and differences between classes can be attributed to the intricate interplay between hydro-meteorological variables (Fig. 7). Classes 3 and 4 have relatively higher sensitivity of peak SWE to temperature thresholds for rain-snow partitioning (Fig. 5b). This can be attributed to relatively higher winter precipitation in these classes coinciding with winter temperatures near 0 °C (Fig. 7a and 7c), where the precipitation form can be rain or snow depending on other environmental factors (Jennings et al., 2018). However, the annual precipitation and winter precipitation ratios are lower in class 4 compared to class 3 because the grids are located on the rain-shadow side of the cascades (Fig. 5a). Moreover, they also have colder average winter (nov-jan) temperatures (−3.35 °C). Hence, the level of sensitivity to Tsmax was relatively lower in class 4 compared to class 3 (Fig. 5b).

Class 1 and 2 regions exhibit distinctly colder winters (Fig. 7c) and are characterized by a more uniform distribution of precipitation throughout the year (Fig. 7a). Notably, as compared to other classes, the precipitation pattern in these areas include higher late spring and early summer precipitation, and delayed runoff coinciding with higher radiation levels. The high sensitivity of peak SWE to the new snow's albedo and albedo decay parameter during the melt phase can be attributed to this delayed precipitation and runoff (Fig. 7a and 7b). Additionally, for the majority of the winter precipitation time frame, the grids in these classes experience cold temperatures well below the rain-snow transition around 0 °C (Fig. 7a and 7c). This explains why peak SWE has low sensitivity to rain-snow partitioning temperature threshold and is more sensitive to albedo parameters in these classes (Fig. 5b).

4. Discussion

Our results indicate that (i) VIC-CropSyst modeled peak SWE and snow duration show relatively higher sensitivities to only a small subset of parameters (two to four out of eleven) (Fig. 3a and 4a), (ii) the key parameters are different across the two target variables (Fig. 3a and 4a), and (iii) elevation, topography and associated temperature and precipitation effects, the timing of precipitation patterns, and the interaction across these variables together with radiation availability (Figs. 6 and 7) results in similarities and differences in sensitivity response across the study domain with two broad clusters of response (Fig. 5). While there is limited similar work for comparison, our results are consistent with prior work in some respects with discrepancies in others, as elaborated below.

The sensitivity of VIC-CropSyst modeled peak SWE and snow duration to a relatively small number of parameters is consistent with previous VIC model studies in other watersheds (e.g., Sepúlveda et al. (2022) in Chile; Bennett et al., (2018) in the Colorado River basin). This is also consistent with the VIC model's streamflow showing sensitivity to a limited number of parameters (e.g., Sepúlveda et al. (2022) in Chile; Mendoza et al., 2015 in the Colorado River basin; Melsen et al., 2016 in Switzerland; Wi et al., 2017 in the American River basin, USA; Gou et al., 2020 in multiple catchments in China). While the literature has used the terminology "*overparameterization in the model*" to describe the lack of relative sensitivity for the majority of parameters (e.g., Demaria et al., 2007; Sepúlveda et al., 2022), we refrain from using that terminology in the context of biophysical models such as VIC-CropSyst or VIC for the

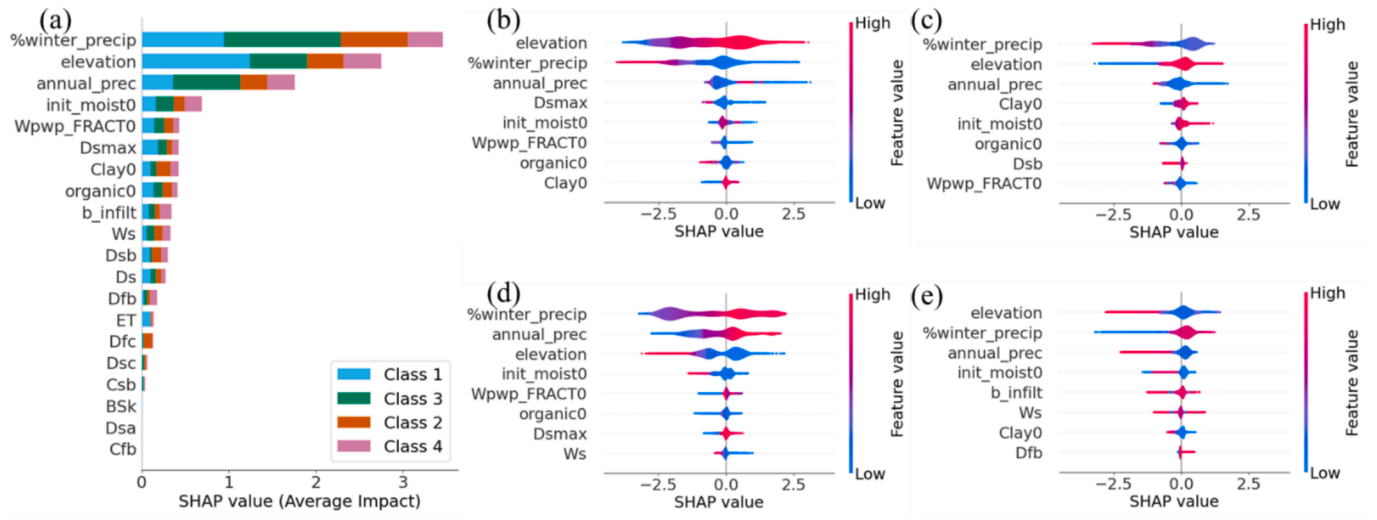


Fig. 6. (a) Absolute SHAP values averaged across the grids within each class, indicating the relative importance of the 21 features in assigning class membership. The sign and level of influence of features for (b) Class 1 (blue), (c) Class 2 (orange), (d) Class 3 (cyan), and (e) Class 4 (pink). Each point in plots (b) through (e) corresponds to a grid. A positive SHAP value for a grid for a particular feature and class indicates that the feature played a positive role in assigning the grid to that class. On the flip side, a negative SHAP value indicates that the feature played a negative role and contributed to not assigning the grid to that class. The colors correspond to the feature's relative magnitude. The height of the violin plot corresponds to the density of the grids.

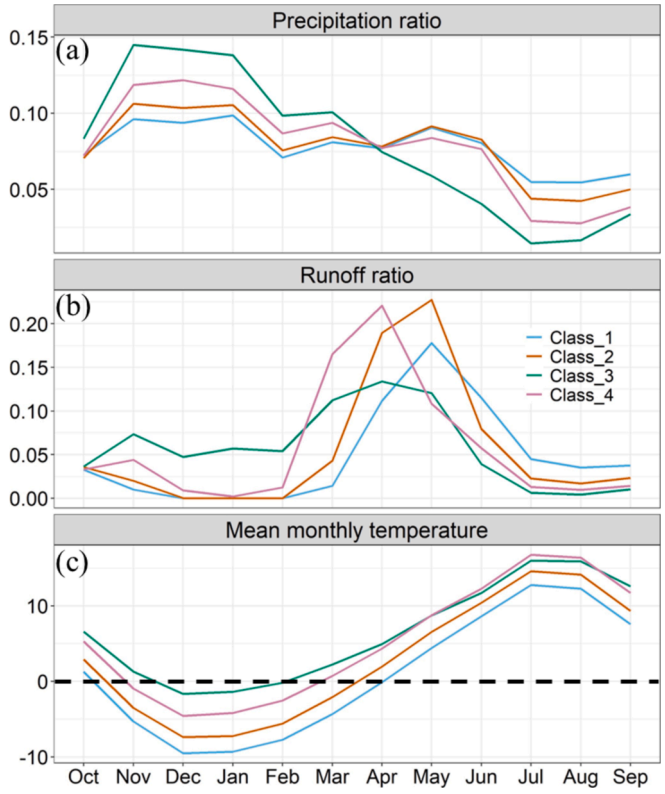


Fig. 7. Line plot showing the median monthly values of three hydro-meteorological variables for the four classes identified using unsupervised K-means clustering. (a) Precipitation ratio (monthly precipitation/total annual precipitation), (b) runoff ratio (monthly runoff/total annual runoff), and (c) mean monthly temperature (°C).

following reasons. First, unlike empirical models, parameters in bio-physical models describe a physical function, and therefore cannot be simply removed. Second, first-order sensitivities are indicative of relative sensitivities and cannot be interpreted as the target variable having no variation to changes in the parameter. Rather, it is just a much lower variation as compared to other parameters. Additionally, key parameters can vary by target variable and the region of analysis, as noted later in this discussion. Therefore, the lack of relative sensitivity in one context cannot be generalized as overparameterization in the model.

Our two target variables (peak SWE and snow duration) were sensitive to different sets of parameters. Peak SWE was primarily sensitive to the temperature thresholds for rain-snow partitioning and the new snow albedo (location dependent; see Fig. 5). In contrast, two albedo parameters (new snow albedo and albedo decay during the melting phase) play a key role in snow duration sensitivity. The variation in key parameters by target variable is consistent with prior work (Bennett et al., 2018a; Chaney et al., 2015; Melsen and Guse, 2021; Sepúlveda et al., 2022; Yeste et al., 2020) and can also be different under climate change (Melsen and Guse, 2021). Geographic differences in the key parameters contributing to peak SWE's sensitivity implies that this information can be utilized in prioritizing new data collection efforts, which can be labor, time and cost-intensive (e.g., airplane flights), only in contexts where it matters.

Inconsistencies in key parameters across studies exist even for the peak SWE variable. This could be for multiple reasons. First is the parameter set considered in the study. For example, Bennett et al. (2018b) and Houle et al. (2017) did not include our key parameter for peak SWE sensitivity – temperature threshold for rain-snow partitioning – in their parameter set and therefore our list of key parameters for peak SWE (Tsmax and NSA) does not match with theirs (winter canopy fraction and winter LAI for Bennett et al., 2018b; albedo decay parameter during melting phase for Houle et al. 2017). The second reason could be the study domain and related dominant hydro-meteorological factors. For example, while Sepúlveda et al. (2022) consider the temperature thresholds for rain-snow partitioning in their parameter set, and peak SWE is sensitive to this parameter, it was not identified as the parameter with the highest relative sensitivity. We find that the rain-snow partitioning parameter has the highest relative sensitivity only in geographic regions where much of the cool-season precipitation co-occurs with near-freezing temperature (Fig. 6a and Fig. 7). Sepúlveda et al. (2022) is focused on watersheds in Chile. Their non-arid watersheds with meaningful precipitation have temperatures well above or below 0 °C during peak precipitation times. Therefore, their precipitation is primarily as either snow or rain, perhaps leading to less relative sensitivity of peak SWE to the precipitation partitioning parameters in their study region.

Even when the study domain has some commonality, we find inconsistencies. For example, our results have some inconsistency with Larabi et al., (2023) for the handful of sub watersheds common between their study domain and ours. While SWE was sensitive to the surface roughness of snowpack and albedo decay coefficient during melt phase across all their watersheds, peak SWE's first order sensitivity to these parameters was negligible in our case. Many factors could lead to this: (a) differences in the sensitivity analysis method (DELSA in our case versus the efficient elementary effects (EEE) screening method used by them) and the parameter thresholds considered, (b) differences in the model itself (e.g., their VIC implementation has a glacial model which our VIC-CropSyst version does not; their rain-snow partitioning method is curvilinear while our is linear; their implementation is at a hydrologic response unit level while our is at a grid-level), and (c) the metric of SWE used.

With respect to snow duration, the key parameters with relatively high sensitivity were the new snow albedo and the albedo decay during the snowmelt phase parameters, consistent with Sepúlveda et al. (2022). While Houle et al. (2017), also has high snow duration sensitivity to the albedo decay during snowmelt, it has relatively less sensitivity to the new snow's albedo. The consistent importance of the albedo decay during melt phase across studies is expected as albedo plays a key role in the energy balance affecting snowmelt (Etchevers et al., 2004) and, therefore snow duration.

In terms of explaining the differences in sensitivity response, we used an ML wrapper that explains the complex model behavior. Sepúlveda et al. (2022) took a simple spearman correlation approach to identify the key drivers of parametric sensitivity across different hydroclimates. They found that annual rainfall and the aridity index were crucial. While these annual factors matter, we found that the seasonal concurrence of precipitation and temperatures is particularly important near the rain-snow line.

Knowing the key parameters contributing to the sensitivity of peak SWE and snow duration and knowing the drivers of sensitivity response offers benefits in improving model parameterization, model accuracy, and, therefore, stakeholder utility from model applications. First, the results point to which static model parameters we need to prioritize for transitioning to more dynamic representation. For example, one of the most sensitive parameters – temperature threshold for precipitation partitioning – can vary dynamically as a function of environmental conditions such as relative humidity (Jennings et al., 2018). Spatially explicit products for precipitation-phase partitioning (e.g., Jennings et al. (2018)) that also account for temporal variation in meteorological controls, such as relative humidity exist and should be leveraged by the modeling community for immediate transitioning of this static parameter to a dynamic characterization. This transition is applicable not just for the VIC-CropSyst model, but hydrological models in general. Additionally, data-driven AI approaches such as attention models that leverage spatiotemporal correlations (e.g., Thapa et al. (2024)) can provide additional future enhancements to these existing products. Second, given limited resources, the results of sensitivity analysis can help inform data collection efforts to improve parameterizations. For example, in our region, data collection related to the precipitation phase partitioning can focus on the Cascades and lower elevations of the Rockies (classes 3 and 4 in Fig. 5a). Similarly, data collection to inform the albedo parameter for *new* snow can be prioritized for just the colder high-elevation regions of the Rocky Mountains (classes 1 and 2 in Fig. 5a).

Finally, results of sensitivity analysis can also support model calibration efforts. This work and others have demonstrated that the key parameters contributing to sensitivity can vary by target variables relevant to different processes (e.g., snow processes versus streamflow processes). In this context, calibrating for processes rather than one key outcome (e.g., streamflow) becomes relevant (Araya et al., 2023; Guse et al., 2016; Melsen and Guse, 2021; Nemri and Kinnard, 2020). Designing calibration as a multi-objective function focused not only streamflow (Girons Lopez et al., 2020; Yeste et al., 2023) – as is predominantly right now (Carvalho et al., 2022; Dadhwal et al., 2010; Hengade et al., 2018; Rajagopalan et al., 2018; Vegad and Mishra, 2022) – but multiple target variables such as peak SWE, snow duration and streamflow conjunctively can offer benefits. This is even more important in a climate change context where streamflow sensitivities can be altered in changing climate and calibrating to processes rather than one main outcome variable can alleviate these issues of changing sensitivities (Melsen and Guse, 2021).

When undertaking these multi-objective calibrations, high-dimensionality of the parameter space can pose a significant challenge. Variation in parameter sensitivity in the target variable space (Figs. S4 and S6) can be leveraged for customized calibration that provides the best model performance. Sensitivity analysis focused on model performance metrics as target variables can provide useful information to narrow down the parameter and parameter ranges that can offer most benefits in the calibration process (e.g., Yeste et al., 2023).

5. Conclusion

We performed a first-order sensitivity analysis of the VIC-CropSyst model for two target variables (peak SWE and snow duration) and determined that both target variables were sensitive only to a small number of parameters which also varied by target variable. The temperature thresholds for precipitation phase partitioning, and the albedo of new snow were important for peak SWE sensitivity, and albedo of new snow and albedo during the snowmelt phase for the snow duration. Existing data products (e.g., Jennings et al. (2018)) can be immediately employed to transition from static to dynamic spatiotemporal representation of the temperature thresholds for precipitation phase partitioning. Additionally, machine learning workflows (clustering and SHAP analysis) around sensitivity analysis provided insights and explainability of complex model behavior, identifying regions that have similar sensitivity responses, and characterizing the major controls of sensitivity response patterns – the seasonal overlap between the timing of precipitation and runoff (driven by snowmelt) with the temperatures. Moreover, any parameterizations done for climate regions based on similarities in the sensitivity response can be adaptive as the climate changes allowing for space–time substitutions. For example, with warming, if class 2′s response starts resembling the response of class 1, parameters finetuned for class 1 can be substituted for class 2 in the future for better representation.

Within the limited sensitivity analysis studies considering peak SWE and snow duration, we observed some agreement and but also several inconsistencies in the key parameters and levels of sensitivity, highlighting the necessity for more comprehensive global sensitivity analyses across multiple applications, while considering large parameter sets and tailoring the analysis to specific objectives and target variables. Given that the computational costs associated with such analyses are no longer prohibitive, especially when leveraging methodologies like the hybrid local–global Distributed Evaluation of Local Sensitivity Analysis (DELSA; Rakovec et al., 2014) approach, as a community, we should emphasize that such exercises should become a routine component of model applications. This will be critical for better understanding of models and uncertainty in model outputs, for strategizing model improvements and ultimately enhancing decision support for water managers operating in snow-dominated watersheds.

6. Financial support

This work was supported by the USDA-NIFA/NSF AI Research Institutes program, under award No. 2021–67021–35344.

CRediT authorship contribution statement

Bhupinderjeet Singh: Writing – review & editing, Writing – original

draft, Visualization, Methodology, Formal analysis, Data curation, Conceptualization. **Tanvir Ferdousi:** Writing – review & editing, Methodology. **John T. Abatzoglou:** Writing – review & editing, Investigation. **Samarth Swarup:** Writing – review & editing, Investigation. **Jennifer C. Adam:** Writing – review & editing, Investigation. **Kirti Rajagopalan:** Writing – review & editing, Supervision, Resources, Project administration, Methodology, Investigation, Funding acquisition, Conceptualization.

Declaration of competing interest

The authors declare that they have no known competing financial interests or personal relationships that could have appeared to influence the work reported in this paper.

Appendix A. Supplementary data

Supplementary data to this article can be found online at https://doi.org/10.1016/j.jhydrol.2024.132193.

Data and code availability

The VIC-CropSyst model code is available in the following GitHub repository (https://github.com/mingliangwsu/VIC-CropSyst-Package.git). The VICCropSyst model parameters, processed data and analysis and plotting code are accessible at: https://github.com/Bhupinderjeetsingh/Singh_VICModeledSnowsensitivity.

References

Abatzoglou, J.T., 2013. Development of gridded surface meteorological data for ecological applications and modelling. Int. J. Climatol. 33, 121–131.

Andreadis, K.M., Storck, P., Lettenmaier, D.P., 2009. Modeling snow accumulation and ablation processes in forested environments: VIC SNOW MODEL. Water Resour. Res. 45. https://doi.org/10.1029/2008WR007042.

Anghileri, D., Voisin, N., Castelletti, A., Pianosi, F., Nijssen, B., Lettenmaier, D.P., 2016. Value of long-term streamflow forecasts to reservoir operations for water supply in snow-dominated river catchments. Water Resour. Res. 52, 4209–4225. https://doi.org/10.1002/2015WR017864.

Araya, D., Mendoza, P.A., Muñoz-Castro, E., McPhee, J., 2023. Towards robust seasonal streamflow forecasts in mountainous catchments: impact of calibration metric selection in hydrological modeling. Hydrol. Earth Syst. Sci. Discuss. 2023, 1–38.

Beck, H.E., Zimmermann, N.E., McVicar, T.R., Vergopolan, N., Berg, A., Wood, E.F., 2018. Present and future Köppen-Geiger climate classification maps at 1-km resolution. Sci. Data 5, 1–12.

Bennett, K.E., Bohn, T.J., Solander, K., McDowell, N.G., Xu, C., Vivoni, E., Middleton, R. S., 2018a. Climate-driven disturbances in the San Juan River sub-basin of the Colorado River. Hydrol. Earth Syst. Sci. 22, 709–725.

Bennett, K.E., Urrego Blanco, J.R., Jonko, A., Bohn, T.J., Atchley, A.L., Urban, N.M., Middleton, R.S., 2018b. Global sensitivity of simulated water balance indicators under future climate change in the colorado basin. Water Resour. Res. 54, 132–149. https://doi.org/10.1002/2017WR020471.

Bhend, J., Bathols, J., Hennessy, K., 2012. Climate change impacts on snow in Victoria. Aspendale Aust. CSIRO Rep. Vic. Dep. Sustain. Environ. 42.

Carvalho, V.S., da Cunha, Z.A., Alvarenga, L.A., Beskow, S., de Mello, C.R., Martins, M. A., de Oliveira, C., de, M., 2022. Assessment of land use changes in the Verde River basin using two hydrological models. J. South Am. Earth Sci. 118, 103954.

Chaney, N.W., Herman, J.D., Reed, P.M., Wood, E.F., 2015. Flood and drought hydrologic monitoring: the role of model parameter uncertainty. Hydrol. Earth Syst. Sci. 19, 3239–3251.

Clark, M.P., Nijssen, B., Lundquist, J.D., Kavetski, D., Rupp, D.E., Woods, R.A., Freer, J. E., Gutmann, E.D., Wood, A.W., Brekke, L.D., Arnold, J.R., Gochis, D.J., Rasmussen, R.M., 2015. A unified approach for process-based hydrologic modeling: 1. Modeling Concept. Water Resour. Res. 51, 2498–2514. https://doi.org/10.1002/2015WR017198.

Dadhwal, V.K., Aggarwal, S.P., Mishra, N., 2010. Hydrological simulation of Mahanadi river basin and impact of land use/land cover change on surface runoff using a macro scale hydrological model. na.

Dang, T.D., Chowdhury, A.K., Galelli, S., 2020. On the representation of water reservoir storage and operations in large-scale hydrological models: implications on model parameterization and climate change impact assessments. Hydrol. Earth Syst. Sci. 24, 397–416.

Darcy, H., 1856. The public fountains of the city of Dijon. Victor Dalmont Paris Fr.

Demaria, E.M., Nijssen, B., Wagener, T., 2007. Monte Carlo sensitivity analysis of land surface parameters using the Variable Infiltration Capacity model. J. Geophys. Res. Atmospheres 112.

Dorman, J.L., Sellers, P.J., 1989. A global climatology of albedo, roughness length and stomatal resistance for atmospheric general circulation models as represented by the simple biosphere model (SiB). J. Appl. Meteorol. Climatol. 28, 833–855.

Elsner, M.M., Cuo, L., Voisin, N., Deems, J.S., Hamlet, A.F., Vano, J.A., Mickelson, K.E.B., Lee, S.-Y., Lettenmaier, D.P., 2010. Implications of 21st century climate change for the hydrology of Washington State. Clim. Change 102, 225–260. https://doi.org/10.1007/s10584-010-9855-0.

Etchevers, P., Martin, E., Brown, R., Fierz, C., Lejeune, Y., Bazile, E., Boone, A., Dai, Y.-J., Essery, R., Fernandez, A., 2004. Validation of the energy budget of an alpine snowpack simulated by several snow models (Snow MIP project). Ann. Glaciol. 38, 150–158.

Ferdousi, T., Liu, M., Rajagopalan, K., Adam, J., Adiga, A., Wilson, M., Ravi, S., Vullikanti, A., Marathe, M.V., Swarup, S., 2023. A Machine Learning Framework to Explain Complex Geospatial Simulations: A Climate Change Case Study. Presented at the Winter Simulation Conference.

Fienen, M.N., Doherty, J.E., Hunt, R.J., Reeves, H.W., 2010. Using prediction uncertainty analysis to design hydrologic monitoring networks: Example applications from the Great Lakes water availability pilot project. US Geological Survey.

Forgy, E.W., 1965. Cluster analysis of multivariate data: efficiency versus interpretability of classifications. biometrics 21, 768–769.

Garg, V., Aggarwal, S.P., Gupta, P.K., Nikam, B.R., Thakur, P.K., Srivastav, S.K., Senthil Kumar, A., 2017. Assessment of land use land cover change impact on hydrological regime of a basin. Environ. Earth Sci. 76, 635. https://doi.org/10.1007/s12665-017-6976-z.

Girons Lopez, M., Vis, M.J.P., Jenicek, M., Griessinger, N., Seibert, J., 2020. Assessing the degree of detail of temperature-based snow routines for runoff modelling in mountainous areas in central Europe. Hydrol. Earth Syst. Sci. 24, 4441–4461. https://doi.org/10.5194/hess-24-4441-2020.

Gou, J., Miao, C., Duan, Q., Tang, Q., Di, Z., Liao, W., Wu, J., Zhou, R., 2020. Sensitivity analysis-based automatic parameter calibration of the VIC model for streamflow simulations over China. e2019WR025968 Water Resour. Res. 56. https://doi.org/10.1029/2019WR025968.

Guo, S., Guo, J., Zhang, J., Chen, H., 2009. VIC distributed hydrological model to predict climate change impact in the Hanjiang basin. Sci. China Ser. E Technol. Sci. 52, 3234–3239. https://doi.org/10.1007/s11431-009-0355-2.

Guse, B., Pfannerstill, M., Strauch, M., Reusser, D.E., Lüdtke, S., Volk, M., Gupta, H., Fohrer, N., 2016. On characterizing the temporal dominance patterns of model parameters and processes. Hydrol. Process. 30, 2255–2270. https://doi.org/10.1002/hyp.10764.

Hall, S.A., Whittemore, A., Padowski, J., Yourek, M., Yorgey, G.G., Rajagopalan, K., McLarty, S., Scarpare, F.V., Liu, M., Asante-Sasu, C., Kondal, A., Brady, M., Gustine, R., Downes, M., Callahan, M., Adam, J.C., 2024. Concurrently assessing water supply and demand is critical for evaluating vulnerabilities to climate change. JAWRA J. Am. Water Resour. Assoc. 1752–1688, 13192. https://doi.org/10.1111/1752-1688.13192.

Hamlet, A.F., Elsner, M.M., Mauger, G.S., Lee, S.-Y., Tohver, I., Norheim, R.A., 2013. An overview of the columbia basin climate change scenarios project: approach, methods, and summary of key results. Atmosphere-Ocean 51, 392–415. https://doi.org/10.1080/07055900.2013.819555.

He, M., Hogue, T.S., Franz, K.J., Margulis, S.A., Vrugt, J.A., 2011. Characterizing parameter sensitivity and uncertainty for a snow model across hydroclimatic regimes. Adv. Water Resour. 34, 114–127. https://doi.org/10.1016/j.advwatres.2010.10.002.

Hengade, N., Eldho, T.I., Ghosh, S., 2018. Climate change impact assessment of a river basin using CMIP5 climate models and the VIC hydrological model. Hydrol. Sci. J. 63, 596–614. https://doi.org/10.1080/02626667.2018.1441531.

Horton, R.E., 1933. The Rôle of infiltration in the hydrologic cycle. Trans. Am. Geophys. Union 14, 446. https://doi.org/10.1029/TR014i001p00446.

Houle, E.S., Livneh, B., Kasprzyk, J.R., 2017. Exploring snow model parameter sensitivity using Sobol'variance decomposition. Environ. Model. Softw. 89, 144–158.

Jennings, K.S., Winchell, T.S., Livneh, B., Molotch, N.P., 2018. Spatial variation of the rain–snow temperature threshold across the Northern Hemisphere. Nat. Commun. 9, 1148.

Karimi, T., Reed, P., Malek, K., Adam, J., 2022. Diagnostic framework for evaluating how parametric uncertainty influences agro-hydrologic model projections of crop yields under climate change. Water Resour. Res. 58. https://doi.org/10.1029/2021WR031249 e2021WR031249.

Krysanova, V., Hattermann, F.F., 2017. Intercomparison of climate change impacts in 12 large river basins: overview of methods and summary of results. Clim. Change 141, 363–379. https://doi.org/10.1007/s10584-017-1919-y.

Larabi, S., Mai, J., Schnorbus, M., Tolson, B.A., Zwiers, F., 2023. Towards reducing the high cost of parameter sensitivity analysis in hydrologic modeling: a regional parameter sensitivity analysis approach. Hydrol. Earth Syst. Sci. 27, 3241–3263.

Lawrence, D.M., Oleson, K.W., Flanner, M.G., Thornton, P.E., Swenson, S.C., Lawrence, P.J., Zeng, X., Yang, Z.-L., Levis, S., Sakaguchi, K., Bonan, G.B., Slater, A. G., 2011. Parameterization improvements and functional and structural advances in Version 4 of the Community Land Model: Parameterization improvements and functional and structural advances. J. Adv. Model. Earth Syst. 3, n/a-n/a. https://doi.org/10.1029/2011MS00045.

Lee, S.-Y., Hamlet, A.F., Fitzgerald, C.J., Burges, S.J., 2011. Methodology for Developing Flood Rule Curves Conditioned on El Niño-Southern Oscillation Classification1: Methodology for Developing Flood Rule Curves Conditioned on El Niño-Southern Oscillation Classification. JAWRA J. Am. Water Resour. Assoc. 47, 81–92. https://doi.org/10.1111/j.1752-1688.2010.00490.x.

Li, D., Wrzesien, M.L., Durand, M., Adam, J., Lettenmaier, D.P., 2017. How much runoff originates as snow in the western United States, and how will that change in the

future? Geophys. Res. Lett. 44, 6163–6172. https://doi.org/10.1002/2017GL073551.
Liang, X., Guo, J., 2003. Intercomparison of land-surface parameterization schemes: sensitivity of surface energy and water fluxes to model parameters. J. Hydrol. 279, 182–209.
Liang, X., Lettenmaier, D.P., Wood, E.F., Burges, S.J., 1994. A simple hydrologically based model of land surface water and energy fluxes for general circulation models. J. Geophys. Res. Atmospheres 99, 14415–14428.
Lilhare, R., Pokorny, S., Déry, S.J., Stadnyk, T.A., Koenig, K.A., 2020. Sensitivity analysis and uncertainty assessment in water budgets simulated by the variable infiltration capacity model for Canadian subarctic watersheds. Hydrol. Process. 34, 2057–2075. https://doi.org/10.1002/hyp.13711.
Livneh, B., Rosenberg, E.A., Lin, C., Nijssen, B., Mishra, V., Andreadis, K.M., Maurer, E. P., Lettenmaier, D.P., 2013. A long-term hydrologically based dataset of land surface fluxes and states for the conterminous United States: Update and extensions. J. Clim. 26, 9384–9392.
Lundberg, S.M., Lee, S.-I., 2017. A unified approach to interpreting model predictions. Adv. Neural Inf. Process. Syst. 30.
Lundberg, S.M., Erion, G., Chen, H., DeGrave, A., Prutkin, J.M., Nair, B., Katz, R., Himmelfarb, J., Bansal, N., Lee, S.-I., 2020. From local explanations to global understanding with explainable AI for trees. Nat. Mach. Intell. 2, 56–67.
Malek, K., Stöckle, C., Chinnayakanahalli, K., Nelson, R., Liu, M., Rajagopalan, K., Barik, M., Adam, J.C., 2017. VIC–CropSyst-v2: A regional-scale modeling platform to simulate the nexus of climate, hydrology, cropping systems, and human decisions. Geosci. Model Dev. 10, 3059–3084. https://doi.org/10.5194/gmd-10-3059-2017.
Maurer, E.P., Wood, A.W., Adam, J.C., Lettenmaier, D.P., Nijssen, B., 2002. A long-term hydrologically based dataset of land surface fluxes and states for the conterminous United States. J. Clim. 15, 3237–3251.
Maxwell, R.M., Miller, N.L., 2005. Development of a coupled land surface and groundwater model. J. Hydrometeorol. 6, 233–247.
Mazrooei, A., Sankarasubramanian, A., Wood, A.W., 2021. Potential in improving monthly streamflow forecasting through variational assimilation of observed streamflow. J. Hydrol. 600, 126559.
Melsen, L.A., Guse, B., 2019. Hydrological Drought Simulations: How Climate and Model Structure Control Parameter Sensitivity. Water Resour. Res. 55, 10527–10547. https://doi.org/10.1029/2019WR025230.
Melsen, L.A., Guse, B., 2021. Climate change impacts model parameter sensitivity–implications for calibration strategy and model diagnostic evaluation. Hydrol. Earth Syst. Sci. 25, 1307–1332.
Melsen, L., Teuling, A., Torfs, P., Zappa, M., Mizukami, N., Clark, M., Uijlenhoet, R., 2016. Representation of spatial and temporal variability in large-domain hydrological models: case study for a mesoscale pre-Alpine basin. Hydrol. Earth Syst. Sci. 20, 2207–2226.
Mendoza, P.A., Clark, M.P., Mizukami, N., Newman, A.J., Barlage, M., Gutmann, E.D., Rasmussen, R.M., Rajagopalan, B., Brekke, L.D., Arnold, J.R., 2015. Effects of hydrologic model choice and calibration on the portrayal of climate change impacts. J. Hydrometeorol. 16, 762–780.
Mitchell, K.E., Lohmann, D., Houser, P.R., Wood, E.F., Schaake, J.C., Robock, A., Cosgrove, B.A., Sheffield, J., Duan, Q., Luo, L., 2004. The multi-institution North American Land Data Assimilation System (NLDAS): Utilizing multiple GCIP products and partners in a continental distributed hydrological modeling system. J. Geophys. Res. Atmospheres 109.
Murillo, O., Mendoza, P.A., Vásquez, N., Mizukami, N., Ayala, Á., 2022. Impacts of subgrid temperature distribution along elevation bands in snowpack modeling: insights from a suite of andean catchments. Water Resour. Res. 58. https://doi.org/10.1029/2022WR032113 e2022WR032113.
Myneni, R.B., Ramakrishna, R., Nemani, R., Running, S.W., 1997. Estimation of global leaf area index and absorbed PAR using radiative transfer models. IEEE Trans. Geosci. Remote Sens. 35, 1380–1393.
Nemri, S., Kinnard, C., 2020. Comparing calibration strategies of a conceptual snow hydrology model and their impact on model performance and parameter identifiability. J. Hydrol. 582, 124474.
Niu, G.-Y., Yang, Z.-L., Mitchell, K.E., Chen, F., Ek, M.B., Barlage, M., Kumar, A., Manning, K., Niyogi, D., Rosero, E., 2011. The community Noah land surface model with multiparameterization options (Noah-MP): 1. Model description and evaluation with local-scale measurements. J. Geophys. Res. Atmospheres 116.
Ossandón, Á., Rajagopalan, B., Tiwari, A.D., Thomas, T., Mishra, V., 2022. A Bayesian hierarchical model combination framework for real-time daily ensemble streamflow forecasting across a rainfed river basin. Earths Future 10. https://doi.org/10.1029/2022EF002958 e2022EF002958.
Qu, Y., Duffy, C.J., 2007. A semidiscrete finite volume formulation for multiprocess watershed simulation. Water Resour. Res. 43. https://doi.org/10.1029/2006WR005752, 2006WR005752.
Rajagopalan, K., Chinnayakanahalli, K.J., Stockle, C.O., Nelson, R.L., Kruger, C.E., Brady, M.P., Malek, K., Dinesh, S.T., Barber, M.E., Hamlet, A.F., 2018. Impacts of near-term climate change on irrigation demands and crop yields in the Columbia River basin. Water Resour. Res. 54, 2152–2182.
Rakovec, O., Hill, M.C., Clark, M.P., Weerts, A.H., Teuling, A.J., Uijlenhoet, R., 2014. Distributed Evaluation of Local Sensitivity Analysis (DELSA), with application to hydrologic models: distributed evaluation of local sensitivity analysis. Water Resour. Res. 50, 409–426. https://doi.org/10.1002/2013WR014063.
Regan, R.S., Markstrom, S.L., Hay, L.E., Viger, R.J., Norton, P.A., Driscoll, J.M., LaFontaine, J.H., 2018. Description of the national hydrologic model for use with the precipitation-runoff modeling system (prms). US Geological Survey.
Richards, L.A., 1931. Capillary conduction of liquids through porous mediums. Physics 1, 318–333.
Rigon, R., Bertoldi, G., Over, T.M., 2006. GEOtop: a distributed hydrological model with coupled water and energy budgets. J. Hydrometeorol. 7, 371–388.
Rosolem, R., Gupta, H.V., Shuttleworth, W.J., Zeng, X., De Gonçalves, L.G.G., 2012. A fully multiple-criteria implementation of the Sobol′ method for parameter sensitivity analysis. J. Geophys. Res. Atmospheres 117. https://doi.org/10.1029/2011JD016355, 2011JD016355.
Saltelli, A., Tarantola, S., Chan, K.-P.-S., 1999. A quantitative model-independent method for global sensitivity analysis of model output. Technometrics 41, 39–56. https://doi.org/10.1080/00401706.1999.10485594.
Saltelli, A., Ratto, M., Andres, T., Campolongo, F., Cariboni, J., Gatelli, D., Saisana, M., Tarantola, S., 2008. Global sensitivity analysis: the primer. John Wiley & Sons.
Schreider, S.Y., Whetton, P.H., Jakeman, A.J., Pittock, A.B., 1997. Runoff modelling for snow-affected catchments in the Australian alpine region, eastern Victoria. J. Hydrol. 200, 1–23.
Sepúlveda, U.M., Mendoza, P.A., Mizukami, N., Newman, A.J., 2022. Revisiting parameter sensitivities in the variable infiltration capacity model across a hydroclimatic gradient. Hydrol. Earth Syst. Sci. 26, 3419–3445.
Singh, A., Mondal, S., Samal, N., Jha, S.K., 2023. Evaluation of precipitation forecasts for five-day streamflow forecasting in Narmada River basin. Hydrol. Sci. J. 68, 161–179. https://doi.org/10.1080/02626667.2022.2151913.
Sobol, I.M., 2001. Global sensitivity indices for nonlinear mathematical models and their Monte Carlo estimates. Math. Comput. Simul. 55, 271–280.
Song, X., Zhang, J., Zhan, C., Xuan, Y., Ye, M., Xu, C., 2015. Global sensitivity analysis in hydrological modeling: Review of concepts, methods, theoretical framework, and applications. J. Hydrol. 523, 739–757.
Staff, S.S., 2014. Natural Resources Conservation Service, United States Department of Agriculture, US General Soil Map (STATSGO2).
Stewart, I.T., Cayan, D.R., Dettinger, M.D., 2004. Changes in snowmelt runoff timing in western North America under a business as usual'climate change scenario. Clim. Change 62, 217–232.
Stöckle, C.O., Donatelli, M., Nelson, R., 2003. CropSyst, a cropping systems simulation model. Eur. J. Agron. 18, 289–307.
Stockle, C.O., Martin, S.A., Campbell, G.S., 1994. CropSyst, a cropping systems simulation model: water/nitrogen budgets and crop yield. Agric. Syst. 46, 335–359.
Tang, Q., Lettenmaier, D.P., 2010. Use of satellite snow-cover data for streamflow prediction in the Feather River Basin, California. Int. J. Remote Sens. 31, 3745–3762. https://doi.org/10.1080/01431161.2010.483493.
Thapa, K.K., Singh, B., Savalkar, S., Fern, A., Rajagopalan, K., Kalyanaraman, A., 2024. Attention-Based Models for Snow-Water Equivalent Prediction, in: Proceedings of the AAAI Conference on Artificial Intelligence. pp. 22969–22975.
Tonkin, M.J., Tiedeman, C.R., Ely, D.M., Hill, C., 2007. OPR-PPR, a computer program for assessing data importance to model predictions using linear statistics. United States Geological Survey-Nevada, Henderson, Nevada.
Treesa, A., Das, J., Umamahesh, N.V., 2017. Assessment of impact of climate change on streamflows using VIC model. Eur Water 59, 61–68.
USDA-NASS. 2016. 2016 Cropland Data Layer. Washington, DC: U.S. Department of Agriculture, National Agricultural Statistics Service. https://nassgeodata.gmu.edu/CropScape/.
Valéry, A., Andréassian, V., Perrin, C., 2014. 'As simple as possible but not simpler': What is useful in a temperature-based snow-accounting routine? Part 1–Comparison of six snow accounting routines on 380 catchments. J. Hydrol. 517, 1166–1175.
Van Werkhoven, K., Wagener, T., Reed, P., Tang, Y., 2008. Characterization of watershed model behavior across a hydroclimatic gradient. Water Resour. Res. 44. https://doi.org/10.1029/2007WR006271, 2007WR006271.
Vegad, U., Mishra, V., 2022. Ensemble streamflow prediction considering the influence of reservoirs in Narmada River Basin, India. Hydrol. Earth Syst. Sci. 26, 6361–6378.
Vertessy, R.A., Dawes, W.R.J., Zhang, L., Hatton, T.J., Walker, J., 1996. Catchment-scale hydrologic modelling to assess the water and salt balance behaviour of eucalypt plantations.
Wainwright, H.M., Finsterle, S., Jung, Y., Zhou, Q., Birkholzer, J.T., 2014. Making sense of global sensitivity analyses. Comput. Geosci. 65, 84–94.
Weerts, A.H., Huisman, J.A., Bouten, W., 2001. Information content of time domain reflectometry waveforms. Water Resour. Res. 37, 1291–1299. https://doi.org/10.1029/2000WR900381.
Wi, S., Ray, P., Demaria, E.M., Steinschneider, S., Brown, C., 2017. A user-friendly software package for VIC hydrologic model development. Environ. Model. Softw. 98, 35–53.
WSDA, 2018. "Washington State Department of Agriculture, Agricultural Land Use Dataset." https://agr.wa.gov/departments/land-and-water/natural-resources/agricultural-land-use.
Yeste, P., Ojeda, M.-G.-V., Gámiz-Fortis, S.R., Castro-Díez, Y., Esteban-Parra, M.J., 2020. Integrated sensitivity analysis of a macroscale hydrologic model in the north of the Iberian Peninsula. J. Hydrol. 590, 125230.
Yeste, P., Rosa-Cánovas, J.J., Romero-Jiménez, E., Ojeda, M.-G.-V., Gámiz-Fortis, S.R., Castro-Díez, Y., Esteban-Parra, M.J., 2021. Projected hydrologic changes over the north of the Iberian Peninsula using a Euro-CORDEX multi-model ensemble. Sci. Total Environ. 777, 146126.
Yeste, P., Melsen, L.A., García-Valdecasas Ojeda, M., Gámiz-Fortis, S.R., Castro-Díez, Y., Esteban-Parra, M.J., 2023. A pareto-based sensitivity analysis and multiobjective calibration approach for integrating streamflow and evaporation data. Water Resour. Res. 59. https://doi.org/10.1029/2022WR033235 e2022WR033235.
Zhao, F., Chiew, F.H., Zhang, L., Vaze, J., Perraud, J.-M., Li, M., 2012. Application of a macroscale hydrologic model to estimate streamflow across southeast Australia. J. Hydrometeorol. 13, 1233–1250.